Supplement of Atmos. Chem. Phys., 22, 10861–10873, 2022
https://doi.org/10.5194/acp-22-10861-2022-supplement

Atmospheric Chemistry and Physics
Open Access

Supplement of

Mixing state of black carbon at different atmospheres in north and southwest China

Gang Zhao et al.

Correspondence to: Min Hu (minhu@pku.edu.cn)

Supplement

1 Measurement site.

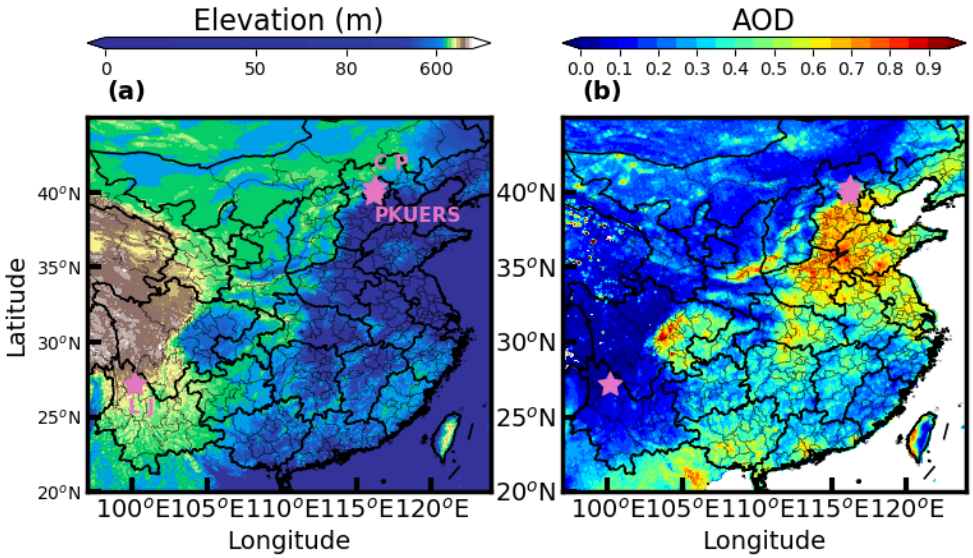

Figure S1: Measurement site of PKUERS, CP, and LJ (marked with stars). Filled colors represent (a) the topography of the Jianghuai Plain. (b) the average aerosol optical depth at 550nm during the year of 2020 from Moderate Resolution Imaging Spectroradiometer onboard satellite Aqua.

2 Instrument setup

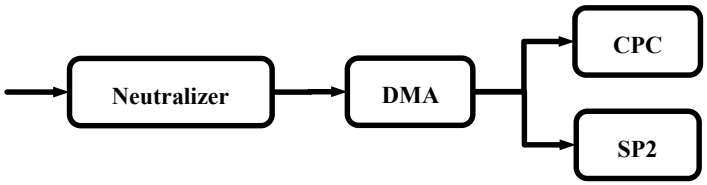

Figure S2. Schematic of the instrument setup for measuring the ambient aerosol RRI.

3 Calculating the coating thickness of BC containing aerosols

In previous SP2 studies, the whole BC diameter (Dp) usually refers to the optically equivalent diameter of the whole particle diameter, which is derived from the Mie calculation with several presumed input parameters (Taylor et al., 2015). Meanwhile, the BC core diameter (Dc) refers to the volume-equivalent diameter (or mass-equivalent diameter) of the BC core by assuming a fixed density for a void-free spherical BC core (1.8 g/cm3 is widely used).

However, the BC cores in ambient BC particles always contain some inside voids and tend to contain more voids in thinly coated BC particles. Thus, using a density of 1.8 g/cm^3 will underestimate the core size and overestimate the coating thickness (and shell = core ratio) to some extent. In this study, with the benefit of the DMA–SP2 coupled system, the Dp can be directly measured by the DMA, which is the mobility diameter of the particle. To derive the Dc, instead of using the fixed density, we applied the closure study suggested by Zhang et al. (2018) to derive the size-dependently effective density for thinly coated BC particles (Fig. S3 for the LJ site) and adopted a density of 1.2 g/cm3 for thickly coated BC particles (Tan et al., 2021).

The multiply charged particles induced by the DMA can be removed by comparing the mobility diameter with the optical diameter derived from the SP2 data. Figure R2 shows the comparison between the mobility diameter and optical diameter of thinly and thickly coated BC for single-charged particles. From Figure S4, the mobility diameter and optical diameter agree well and thus the method above can be used to derive the coating thickness of the thinly and coated BC particles. It should be noted here that, when it comes to the BC size distribution, the mass-equivalent diameter of BC cores (assuming a density of 1.8 g/cm3) was adopted in this study for direct comparison with previous studies.

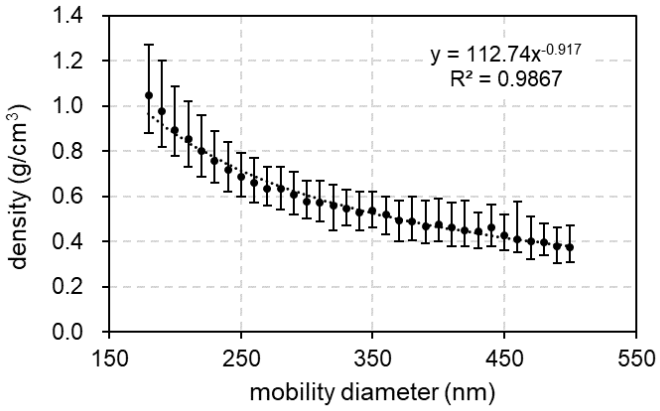

Figure S3. Size-dependently effective density of the BC core for thinly-coated BC particles.

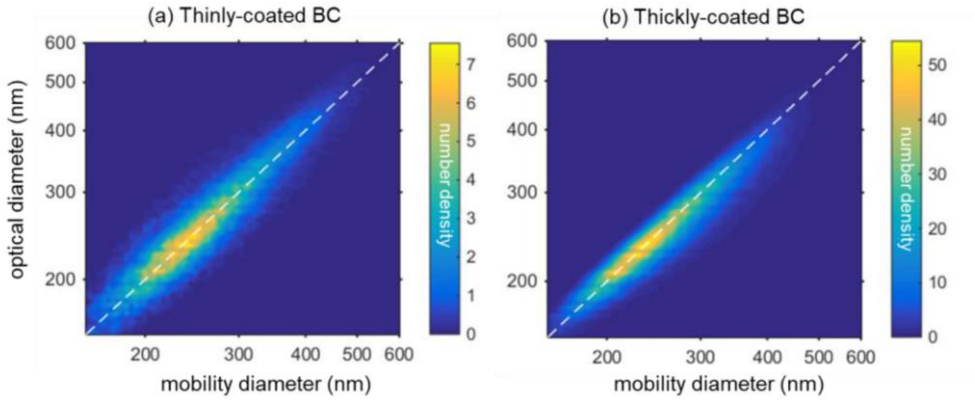

Figure S4. Comparison between optical diameter and mobility diameter for (a) thinly-coated BC and (b) thickly-coated BC.

4 Distinguish the BC particles as coated type and attached type

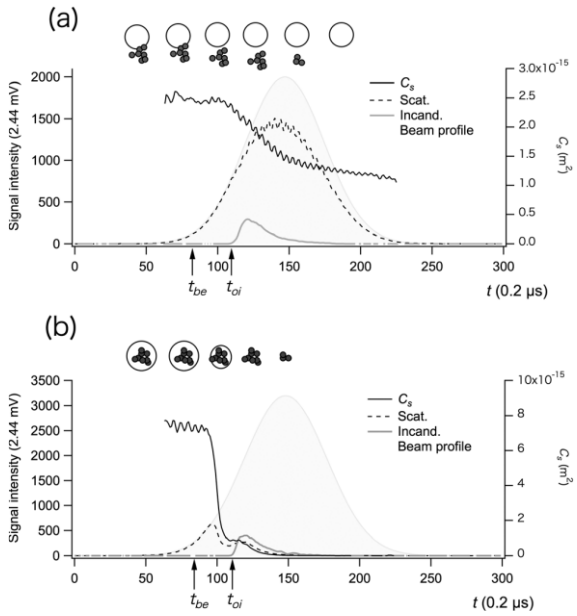

Figure S5. The scattering and incandesce signals for (a) attached and (b) coated particles. The Cs represent the calculated time series of the scattering cross-section. The Beam profile denotes the theoretically calculated scattering signals if the non-BC components were not evaporated.

Figure. S5 gives examples of the measured scattering and incandensce signals for attached and coated particles. For the coated type, all of the coating material will evaporate and the scattering cross-sections will decrease to zero after passing through the laser beam, while the scattering cross-section of the attached BC-containing aerosol will not decrease to zero. Firstly, the beam profile, which indicates the theoretically calculated light scattering time series with the assumption that the coating material would not evaporate when passing through the laser beam. Then the corresponding scattering cross-section time series were calculated (C_s in fig. S5) by comparing the measured scattering signal time series (Scat. In fig.S5) and the calculated

beam profile using the method of Dahlkötter et al. (2014). These particles are sorted as the attached BC ones when the mean C_s values, of which the time range corresponds to the 10% tail of the beam profile, were larger than 5% of the maximum value of C_s.

5 Overview of the measurement results for the PKU site.

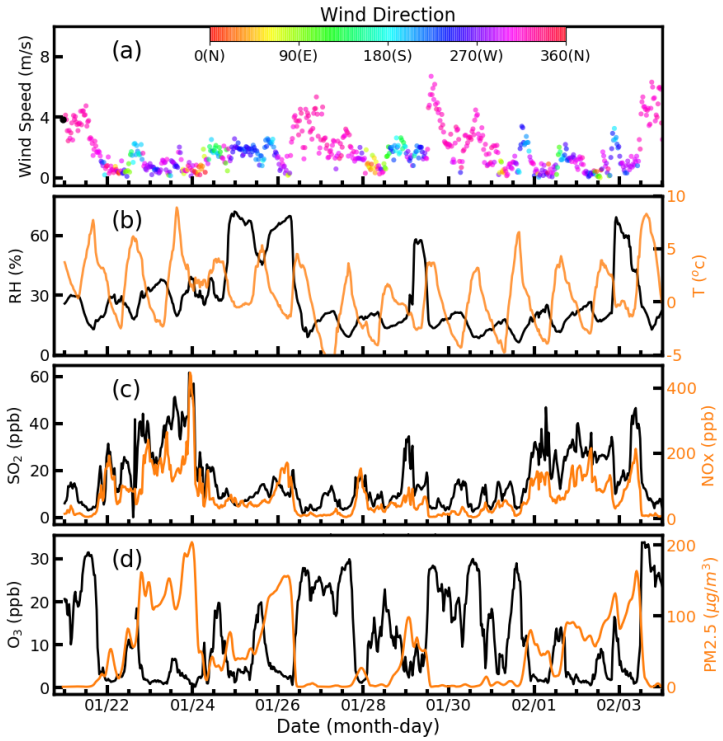

Figure. S6. The time series of (a) wind speed, (b) RH (in black), and T (in orange), (c) chemical compositions of organic compositions (green), nitrate (blue), sulfate (red), ammonium (orange), and chlorine (purple), (d) SO_2 (black) and NOx (orange), and (3) O_3 (black) and $PM_{2.5}$ (orange) during the measurement conducted at PKU. The filled colors in panel (a) represent the wind directions.

6 Overview of the measurement results for the CP site.

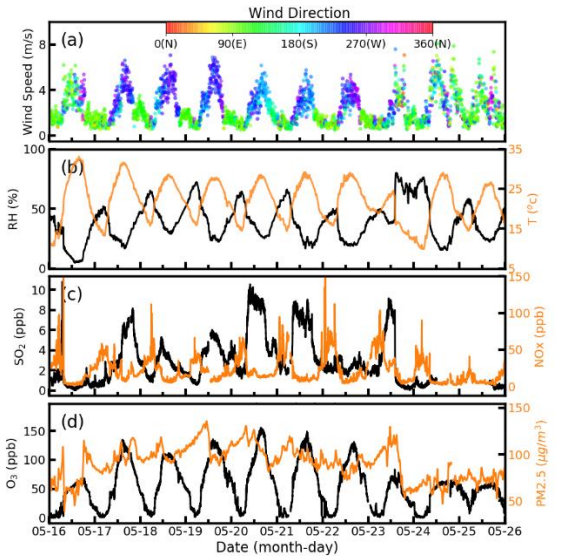

Figure. S7. The time series of (a) the wind speed, (b) RH (in black), and T (in orange), (c) chemical compositions of organic compositions (green), nitrate (blue), sulfate (red), ammonium (orange), and chlorine (purple), (d) SO_2 (black) and NOx (orange), and (3) O3 (black) and $PM_{2.5}$ (orange) during the measurement conducted at CP. The filled colors in panel (a) represent the wind directions.

7 Overview of the measurement results for the LJ site.

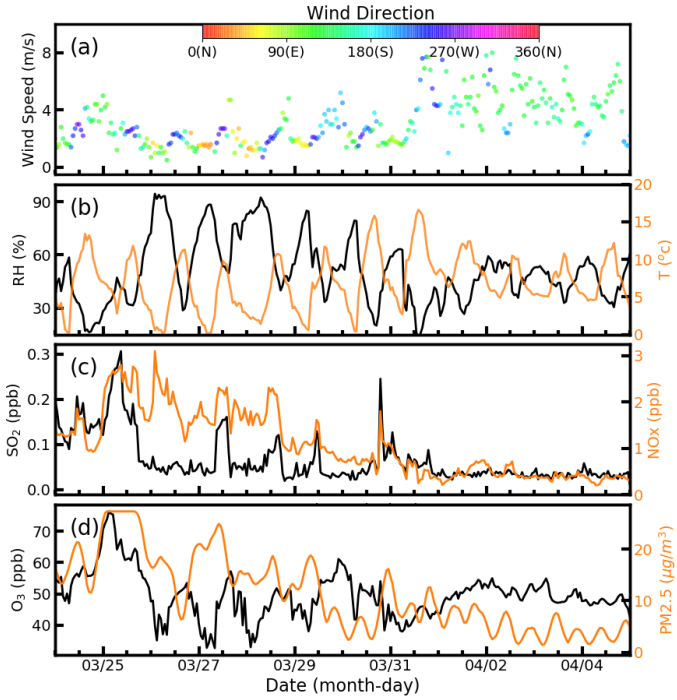

Figure. S8. The time series of (a) wind speed, (b) RH (in black), and T (in orange), (c) chemical compositions of organic compositions (green), nitrate (blue), sulfate (red), ammonium (orange), and chlorine (purple), (d) SO_2 (black) and NOx (orange), and (3) O3 (black) and $PM_{2.5}$ (orange) during the measurement conducted at

LJ. The filled colors in panel (a) represent the wind directions.

8 Backtrajectories during the three measurements

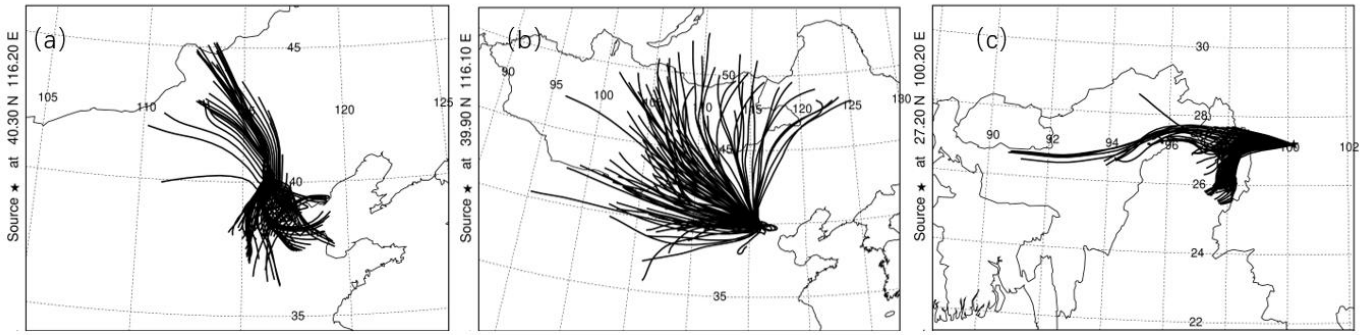

Figure S9. Back trajectories during the measurements at (a) PKU, (b) CP, and (c) LJ sites. The back trajectories were calculated by using the Hybrid Single-Particle Lagrangian Integrated Trajectory (HYSPLIT) model (https://www.ready.noaa.gov/HYSPLIT.php, last access: 19 May 2022).

9 Comparison between the number concentrations of BC and mass concentration of the OA.

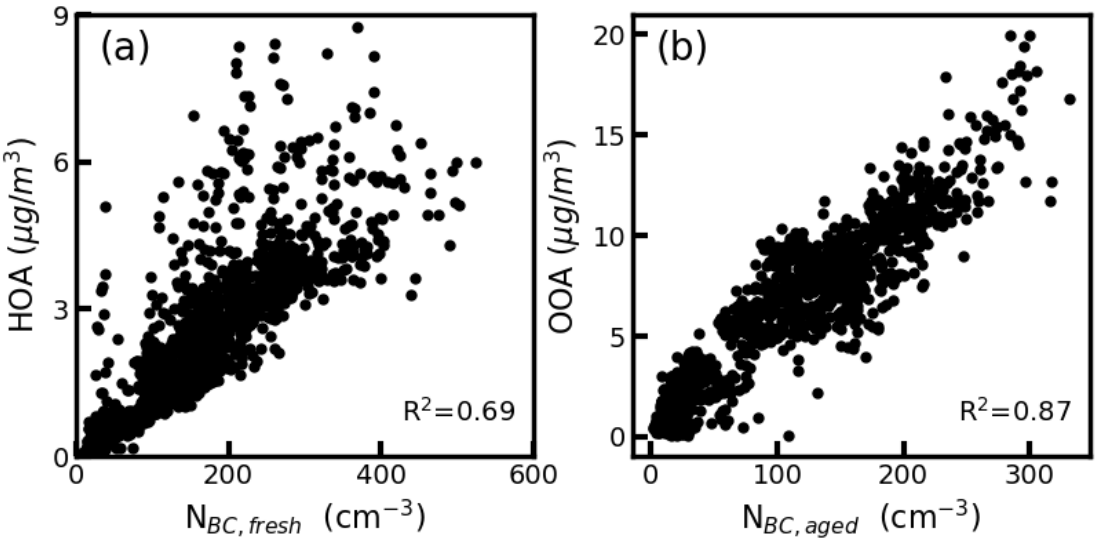

Figure. S10. Comparison between (a) the number concentrations of the fresh BC and the mass concentrations of HOA, and (b) the number concentrations of the aged BC and the mass concentrations of OOA.

References

Ding, S., Liu, D., Zhao, D., Hu, K., Tian, P., Zhou, W., Huang, M., Yang, Y., Wang, F., Sheng, J., Liu, Q., Kong, S., Cui, P., Huang, Y., He, H., Coe, H., and Ding, D.: Size-Related Physical Properties of Black Carbon in the Lower Atmosphere over Beijing and Europe, Environ Sci Technol, 53, 11112-11121, 10.1021/acs.est.9b03722, 2019.

Liu, D., Joshi, R., Wang, J., Yu, C., Allan, J. D., Coe, H., Flynn, M. J., Xie, C., Lee, J., Squires, F., Kotthaus,

S., Grimmond, S., Ge, X., Sun, Y., and Fu, P.: Contrasting physical properties of black carbon in urban Beijing between winter and summer, Atmospheric Chemistry and Physics, 19, 6749-6769, 10.5194/acp-19-6749-2019, 2019.

Tan, T., Hu, M., Du, Z., Zhao, G., Shang, D., Zheng, J., Qin, Y., Li, M., Wu, Y., Zeng, L., Guo, S., and Wu, Z.: Measurement report: Strong light absorption induced by aged biomass burning black carbon over the southeastern Tibetan Plateau in pre-monsoon season, Atmospheric Chemistry and Physics, 21, 8499-8510, 10.5194/acp-21-8499-2021, 2021.

Taylor, J. W., Allan, J. D., Liu, D., Flynn, M., Weber, R., Zhang, X., Lefer, B. L., Grossberg, N., Flynn, J., and Coe, H.: Assessment of the sensitivity of core / shell parameters derived using the single-particle soot photometer to density and refractive index, Atmospheric Measurement Techniques, 8, 1701-1718, 10.5194/amt-8-1701-2015, 2015.

Zhang, Y., Su, H., Ma, N., Li, G., Kecorius, S., Wang, Z., Hu, M., Zhu, T., He, K., Wiedensohler, A., Zhang, Q., and Cheng, Y.: Sizing of ambient particles from a Single Particle Soot Photometer measurement to retrieve mixing state of Black Carbon at a Regional site of the North China Plain, Journal of Geophysical Research: Atmospheres, 123, 12778-12795, doi:10.1029/2018JD028810, 2018.

Ding, S., Liu, D., Zhao, D., Hu, K., Tian, P., Zhou, W., Huang, M., Yang, Y., Wang, F., Sheng, J., Liu, Q., Kong, S., Cui, P., Huang, Y., He, H., Coe, H., and Ding, D.: Size-Related Physical Properties of Black Carbon in the Lower Atmosphere over Beijing and Europe, Environ Sci Technol, 53, 11112-11121, 10.1021/acs.est.9b03722, 2019.

Liu, D., Joshi, R., Wang, J., Yu, C., Allan, J. D., Coe, H., Flynn, M. J., Xie, C., Lee, J., Squires, F., Kotthaus, S., Grimmond, S., Ge, X., Sun, Y., and Fu, P.: Contrasting physical properties of black carbon in urban Beijing between winter and summer, Atmospheric Chemistry and Physics, 19, 6749-6769, 10.5194/acp-19-6749-2019, 2019.

Tan, T., Hu, M., Du, Z., Zhao, G., Shang, D., Zheng, J., Qin, Y., Li, M., Wu, Y., Zeng, L., Guo, S., and Wu, Z.: Measurement report: Strong light absorption induced by aged biomass burning black carbon over the southeastern Tibetan Plateau in pre-monsoon season, Atmospheric Chemistry and Physics, 21, 8499-8510, 10.5194/acp-21-8499-2021, 2021.

Taylor, J. W., Allan, J. D., Liu, D., Flynn, M., Weber, R., Zhang, X., Lefer, B. L., Grossberg, N., Flynn, J., and Coe, H.: Assessment of the sensitivity of core / shell parameters derived using the single-particle soot photometer to density and refractive index, Atmospheric Measurement Techniques, 8, 1701-1718, 10.5194/amt-8-1701-2015, 2015.

Zhang, Y., Su, H., Ma, N., Li, G., Kecorius, S., Wang, Z., Hu, M., Zhu, T., He, K., Wiedensohler, A., Zhang, Q., and Cheng, Y.: Sizing of ambient particles from a Single Particle Soot Photometer measurement to retrieve mixing state of Black Carbon at a Regional site of the North China Plain, Journal of Geophysical Research: Atmospheres, 123, 12778-12795, doi:10.1029/2018JD028810, 2018.